16th Australasian Fluid Mechanics Conference
Crowne Plaza, Gold Coast, Australia
2-7 December 2007

On Flow Structure in an Oscillating-Triangular-Jet Nozzle: Conditionally-Averaged Wall Pressure

S. K. Lee and P. V. Lanspeary

School of Mechanical Engineering
The University of Adelaide, Adelaide, South Australia, 5005 AUSTRALIA

Abstract

A jet flow from a triangular-inlet orifice can be made to oscillate or "precess" by partially confining it with a short cylindrical chamber. However, for a narrow range of chamber lengths, the jet is deflected but does not oscillate. Earlier flow-visualisation experiments with this stationary-deflected triangular jet (SDTJ) have revealed a complex flow pattern inside the chamber. The aim of this study is to discover by conditional averaging if there is a similar flow pattern in the fully oscillating jet flow.

A backward-facing pressure probe placed in the reattaching-flow region of the chamber surface is used as a detector of jet-flow oscillation. With the signal from this detector and simultaneous wall-pressure measurements, we have obtained conditionally-averaged pressure distributions on the wall of the oscillating-triangular-jet (OTJ) nozzle. The OTJ surface-pressure distributions have the same features as the time-averaged SDTJ surface-pressure distribution, and so the inferred OTJ surface-flow topology has the same features as the SDTJ. However, for the OTJ, the chamber is twice as long, and the conditionally-averaged pressure distribution is much more asymmetrical about a mirror plane drawn through the axis of the nozzle and the detector probe. We conclude that the net radial force due to the asymmetric pressure distribution is large enough to produce significant deflection of the OTJ flow in directions normal to the chamber axis.

Introduction

A device consisting of a circular inlet orifice and a cylindrical chamber with an exit lip (Figure 1) can produce a naturally-oscillating jet flow. This device is known as the "fluidic-precessing-jet" (FPJ) nozzle. Nathan et al. [4] show that, for the FPJ to oscillate reliably, the inlet-expansion ratio (D/d_{e1}) must be larger than about 5.0, and the length ratio of the chamber must be in the range $2.6 \lesssim L/D \lesssim 2.8$. The nozzle is usually made with an exit-lip height of $0.1D$. Nathan's early studies of the FPJ [4] identified several flow features inside the chamber.

1. The first of these features is asymmetric deflection of the jet flow from the inlet orifice, and reattachment of the deflected jet to the side wall of the chamber (Figure 1).
2. There is a circumferential negative-bifurcation line between the path traced by the precessing reattachment point and the inlet plane of the nozzle.
3. There is a torus of strong tangential swirl between the negative-bifurcation line and the inlet plane of the nozzle. The swirling fluid spirals inward and is entrained into the jet flow from the inlet orifice.
4. Fluid entrained into the jet flow is ejected from the chamber. The partial vacuum thus produced induces a reverse flow through the exit plane of the nozzle.

Mi et al. [3] found that an FPJ-like flow oscillation is obtained with a number of different inlet-orifice shapes. In particular, with an equilateral-triangular orifice (Figure 2), oscillation is obtained at much lower expansion ratios than with the FPJ. The oscillating-triangular-jet (OTJ) nozzle therefore has much lower pressure loss than the FPJ nozzle. In a parametric study of the OTJ nozzle, Lee et al. [2] have verified that continuous oscillation occurs at much smaller expansion ratios than for the FPJ.

Lee et al. [1] also observe that, for a narrow range of nozzle geometries ($D/d_{e1} = 3.5$, $1.0 < L/D \lesssim 1.25$), the jet is deflected towards the wall but does not oscillate. In the stationary-deflected flow, "time-averaged" observations capture the effects of jet deflection and only details of turbulence motion are removed. Figure 3(a) is a typical surface-flow image of this "stationary-deflected triangular jet" (SDTJ). The image shows that the SDTJ has the same four features as listed above, but it also reveals new detail. As shown in Figure 3(c), there is a sink focus (F_a, F_b) upstream and on each side of the jet-reattachment node (N). These foci counter rotate and are of unequal size. The reverse flow through the chamber-exit plane is attracted to the larger focus. The surface-flow pattern clearly has no symmetry, and this is a reminder that the instantaneous, time-dependent oscillating-jet flow should also be strongly asymmetric.

The similarities between the OTJ and the SDTJ, and the propensity of the SDTJ to oscillate tempt us to believe that the OTJ flow pattern is much the same as the SDTJ flow pattern, but we need more evidence. Therefore, the aim of the research reported in this paper is to perform conditionally-sampled experiments which record the internal pressure distribution on the wall of the nozzle when the oscillating deflected jet has a specified azimuthal orientation and a specified direction of oscilla-

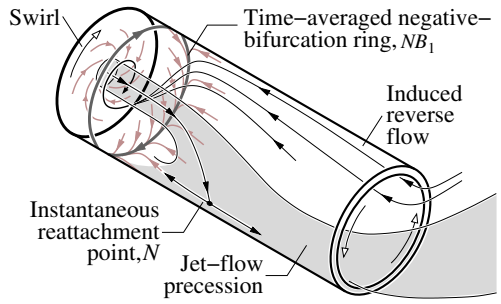

Figure 1: The fluidic-precessing-jet (FPJ) nozzle: typical geometry and early flow-visualisation results.

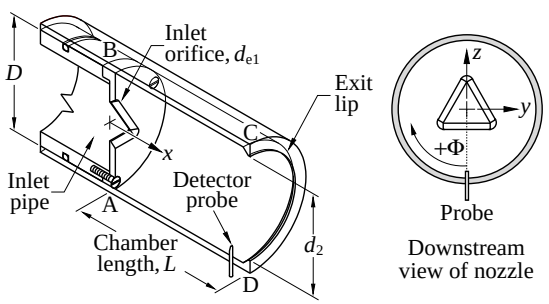

Figure 2: The oscillating-triangular-jet (OTJ) nozzle components and geometric parameters.

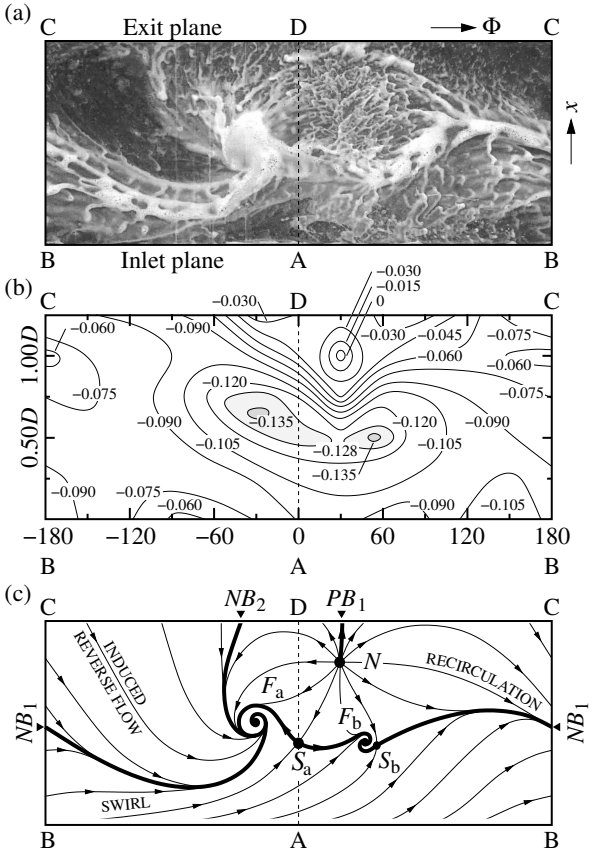

Figure 3: Surface flow for the stationary-deflected triangular jet (SDTJ) from Lee et al. [1]. (a) Paste visualisation. (b) Distribution of static-pressure coefficient. (c) Streakline interpretation.

tion. A backward-facing pressure transducer detects the desired azimuthal orientation of the jet. The direction of oscillation is determined by seeding the flow with air bubbles and by directly observing the flow. From the new data we obtain conditionally-averaged pressure on the wall of the OTJ chamber.

Apparatus

Figure 2 shows the OTJ nozzle used for this study. The nozzle has an internal chamber diameter D. Flow enters the nozzle through an equilateral-triangular orifice with an equivalent diameter of $d_{e1} = D/3.5$, and it leaves the chamber through a lip of diameter $d_2 = 0.9D$. The length-to-diameter ratio (L/D) of the chamber is 2.50, and the inlet-orifice Reynolds number is $Re_1 = d_{e1}U_1/\nu = 70,000$.

As shown in Figures 4 and 5, the OTJ nozzle is submerged in a tank of water. The OTJ nozzle is connected to a smooth-

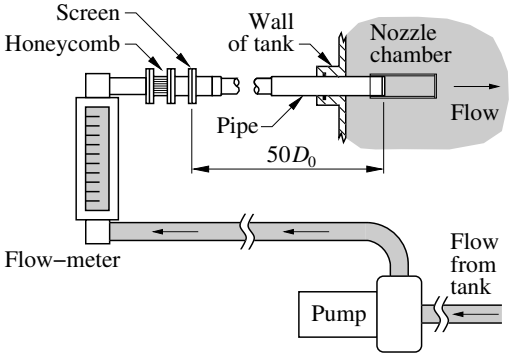

Figure 4: Flow circuit showing major components.

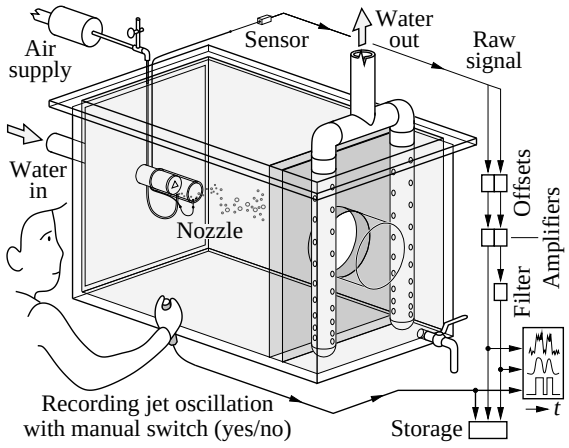

Figure 5: Arrangement of equipment for simultaneous air-bubble visualisation and pressure measurements in the OTJ flow.

wall tube of internal diameter $D_0 = 0.763D$ and length $50D_0$. Flow passes through a honeycomb and wire-mesh screen before entering the tube. The tube provides the OTJ nozzle with inlet-flow conditions which are a close approximation to a fully-developed pipe flow [2]. Flow rate is measured with a 2-inch Fischer & Porter float/tube flowmeter.

Measurements of pressure at the inside surface of the OTJ nozzle are obtained using Codman strain-gauge transducers with a range of ± 166 kPa and a response time of about 0.1 ms. Each transducer sits inside the end of a 2-mm-diameter tube which is bevelled to expose the transducer. One of these pressure probes is used as a detector of azimuthal orientation of the jet flow. The "detector probe" is located in the reattached-flow region of chamber surface just upstream from the exit lip (Figure 2), where it protrudes 3 mm from the surface and is oriented to face the inlet orifice. To obtain the wall-pressure signals, 2-mm tubes which contain the Codman transducers are flush-mounted in the wall of the chamber.

For conditional averaging, the signal from the detector probe is converted into a boolean sequence by passing it through a comparator. Typical signals from the detector probe and the comparator are shown in Figure 6. The low-to-high and high-to-low transition levels of the comparator are adjusted so that the comparator detects the same number of jet oscillations as are directly observed when the flow is seeded with air bubbles.

Wall-Pressure Distribution of Stationary-Deflected Jet

Figure 3(b) shows the wall-pressure distribution of the stationary-deflected jet. Figure 3(b) is useful because it provides a necessary link between the SDTJ surface-flow pattern (Figure 3(c)) and the conditionally-averaged wall-pressure distribution of the OTJ flow. The SDTJ pressure distribution is

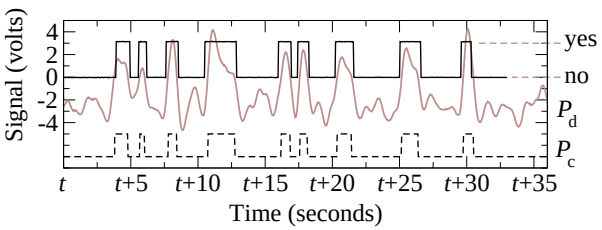

Figure 6: Comparison of detector-probe signal (P_d), output of calibrated comparator (dashed line, P_c) and directly observed alignment of flow reattachment with the detector probe (solid line, yes/no).

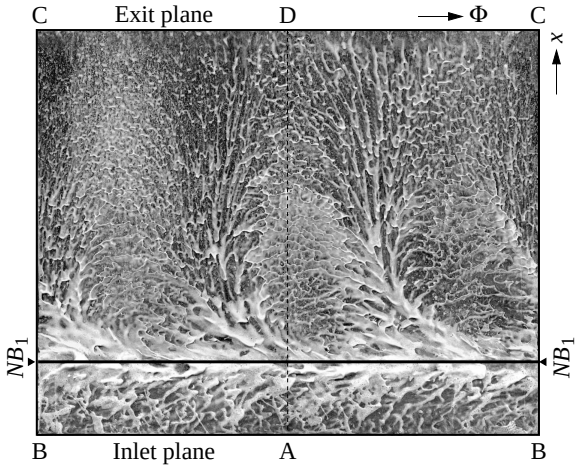

Figure 7: Time-averaged surface-flow visualisation pattern in the OTJ chamber by Lee et al. [1]. Negative-bifurcation line is labelled NB_1. $D/d_{e1}=3.5$, $L/D=2.50$, $Re_1=70,000$.

asymmetric, and it contains a region of maximum pressure at the jet-reattachment node. Closer to the inlet plane and to each side of this pressure maximum, there are two regions of minimum pressure which, according to flow visualisation, are sink foci. These pressure minima (sink foci) are of unequal size. The results (Figure 3) are obtained from time-averaged flow visualisation and time-averaged pressure measurements. However, as in Figure 7, using the same experimental techniques in an oscillating-jet flow obliterates most of the important features in the surface-flow visualisation and in the pressure distribution. We therefore choose to estimate an instantaneous wall-pressure distribution by cross-correlation of an event-detector (or reference) signal with wall-pressure signals from elsewhere on the cylindrical surface of the OTJ nozzle. This leads to a conditionally-averaged pressure which is an approximation to the phase-averaged surface-pressure distribution in the OTJ chamber.

Conditionally-Averaged Wall Pressure of Oscillating Jet

The conditionally-averaged pressure on the internal cylindrical surface of the OTJ nozzle is defined as the cross correlation

$$P_{wc}(x,\Phi)=\frac{\overline{P_w(x,\Phi,t)\,P_c(t)}}{\overline{P_c(t)}}\ , \qquad (1)$$

where P_w is the fluctuating component of wall pressure, and P_c is the comparator output from a single detector probe at $(x,\Phi)=(L-0.30D,0)$. Azimuth angle Φ and distance x from the inlet are defined in Figure 2. Signals from the wall-pressure probe (P_w) and from the detector probe (P_c) are amplified and low-pass filtered at a cut-off frequency of 0.9 Hz. The signals are recorded with a wall-pressure probe located at each of the 107 grid points shown in Figure 8. There are about 80 oscillation events during each 4-minute recording period. The conditionally-averaged pressure is plotted in Figure 8 as pressure coefficient, P_{wc}/q_1, where q_1 is the dynamic pressure of the mean flow through the inlet orifice. The location of the detector probe, at $(x,\Phi)=(2.20D,0)$, is marked with a "•" symbol.

The conditionally-averaged pressure distribution in Figure 8 is asymmetric about the line $\overline{AD}$ (i.e. $\Phi=0$). The large region of maximum pressure centred at $(x,\Phi)\approx(1.25D,30^\circ)$ is evidence of a reattaching jet. This is shown as flow-feature ① in the thumbnail sketches in Figure 8. The pair of large-scale pressure minima near $(x,\Phi)\approx(1.40D,-130^\circ)$ is interpreted as a surface-sink vortex (flow-feature ②). The conditionally-

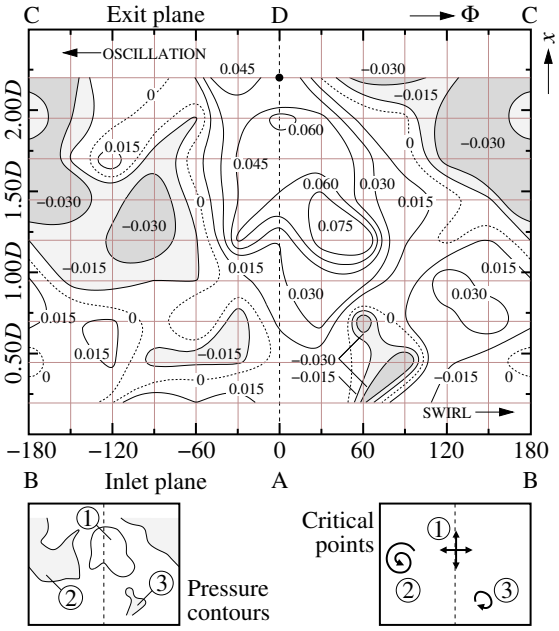

Figure 8: Conditionally-averaged static pressure on oscillating-triangular-jet (OTJ) chamber wall; pressure coefficient, P_{wc}/q_1. The detector probe (•) is $0.30D$ upstream from point D. Direction of the jet oscillation and the swirl are observed by seeding the flow with air bubbles. $D/d_{e1}=3.5$, $L/D=2.50$, $Re_1=70,000$.

averaged pressure distribution in Figure 8 also contains a number of closed contours or "ridges" which are smaller or narrower than the grid-point spacing. Attempts to identify these features as "outliers" by applying the normalised-median test of Westerweel and Scarano [6] are unsuccessful, and so we propose to modify the conditional-averaging method.

Theoretical Basis of the Modified Phillips Method

In their study of extreme ocean waves, Phillips et al. [5] show that it is possible to obtain a reliable estimate of the surface-displacement $\overline{\zeta}$ surrounding an extreme wave crest by using a simple autocorrelation. The height of the extreme wave is a rare event and displacement during this event exceeds the overall r.m.s. surface displacement ζ' by a factor $\gamma\gg1$ (i.e. $\zeta\gg\zeta'$). The r.m.s. surface displacement is uniform over a random sea. By assuming that surface height displacement has a Gaussian probability density function, Phillips showed that the expected surface displacement near an extreme wave crest is given approximately by the following expression:

$$\begin{array}{ccc}\text{dimensionless height distribution} & = & \text{autocorrelation of surface displacement}\\ \dfrac{\overline{\zeta(\vec{x}+\vec{r},t)}}{\overline{\zeta(\vec{x},t)}_{\zeta>\gamma\zeta'}} & = & R_{\zeta\zeta}(\vec{r}),\end{array} \qquad (2)$$

where vector $\vec{r}$ is displacement from the crest, which is at $\vec{r}=0$. The $\overline{\zeta}$ notation indicates averaging over space $\vec{x}$ and/or time t. The space-time autocorrelation function of surface displacement is

$$R_{\zeta\zeta}(\vec{r})=\frac{\overline{\zeta(\vec{x}+\vec{r},t)\,\zeta(\vec{x},t)}}{\zeta'(\vec{x}+\vec{r},t)\,\zeta'(\vec{x},t)}\ . \qquad (3)$$

In the OTJ flow field, the extreme event occurs at the time when the jet flow impinges on the detector probe and the jet flow is deflected (downwards) at azimuthal angle $\Phi=0$. It therefore

seems possible that Phillips' method can be used for estimating the wall-pressure distribution during the "extreme" event which indicates a downward deflected jet. However, there are two differences between the Phillips estimate of extreme wave shape, and estimating the conditionally sampled wall-pressure distribution in the OTJ nozzle:

1. Phillips' method uses an *autocorrelation* function of surface displacement. Conditional sampling of OTJ wall pressure requires the *cross-correlation* function of the pressure signal P_d from the detector and the (static) pressure signal P_w on the chamber wall:

$$R_{wd}(x,\Phi) = \frac{\overline{P_w(x,\Phi,t)\,P_d(t)}}{P_w'(x,\Phi,t)\,P_d'(t)}\ , \qquad (4)$$

   where P_w' and P_d' are the r.m.s. pressure signals. The notation $\overline{P_w P_d}$ represents time averaging of $P_w P_d$.

2. The r.m.s. fluctuation of ocean-wave displacement is uniform over the whole field but for the OTJ, the r.m.s. fluctuation of wall pressure is **not** uniform. The pressure distribution, is therefore estimated using

$$P_{wd}(x,\Phi) = R_{wd}(x,\Phi)\times P_w'(x,\Phi,t) = \frac{\overline{P_w(x,\Phi,t)\,P_d(t)}}{P_d'(t)}\ . \qquad (5)$$

   This might be called a "modified Phillips estimate" of the instantaneous wall-pressure distribution due to a deflected OTJ flow.

The Modified Phillips Estimate (MPE) of Wall Pressure

In Figure 9, the MPE of the surface pressure (Equation 5) in the OTJ nozzle is plotted as pressure coefficient, P_{wd}/q_1, where q_1 is dynamic pressure of the mean flow at the inlet.

The MPE (Figure 9(a)) is somewhat like the conditional average (Figure 8) in that the pressure distribution is asymmetric, the pressure contours are aligned in the NW-SE direction[1], and it has a pressure maximum and two pressure minima. The observable differences between the "modified Phillips estimate" of the OTJ wall-pressure distribution (Figure 9(a)) and the SDTJ wall-pressure distribution (Figure 3(b)) are that

1. the OTJ pressure field has greater asymmetry about the line $\overline{\text{AD}}$, which represents the azimuth angle $\Phi = 0$,
2. this larger asymmetry of the OTJ is accompanied by an alignment of pressure contours in the NW-SE direction,
3. the OTJ has a much larger region of low pressure on the "left" side, and
4. this region of low pressure is much further from the line $\overline{\text{AD}}$ (is at $\Phi \approx -130^\circ$ in the OTJ but is at $\Phi \approx -30^\circ$ in the SDTJ).

By visually correlating features in the surface pressure field of Figure 9(a) with "equivalent" features in the SDTJ pressure field (Figure 3(b)) and by suitably modifying Figure 3(c), it is now possible to infer a phase-averaged surface-flow pattern for the OTJ. The inferred surface-flow pattern is shown in Figure 9(b).

In Figure 9(b), the path of the emerging-jet flow is indicated by the positive-bifurcation line PB_1 which extends from the reattachment node N to the exit plane. The OTJ flow, which spreads

[1] Compass North points upwards on the page.

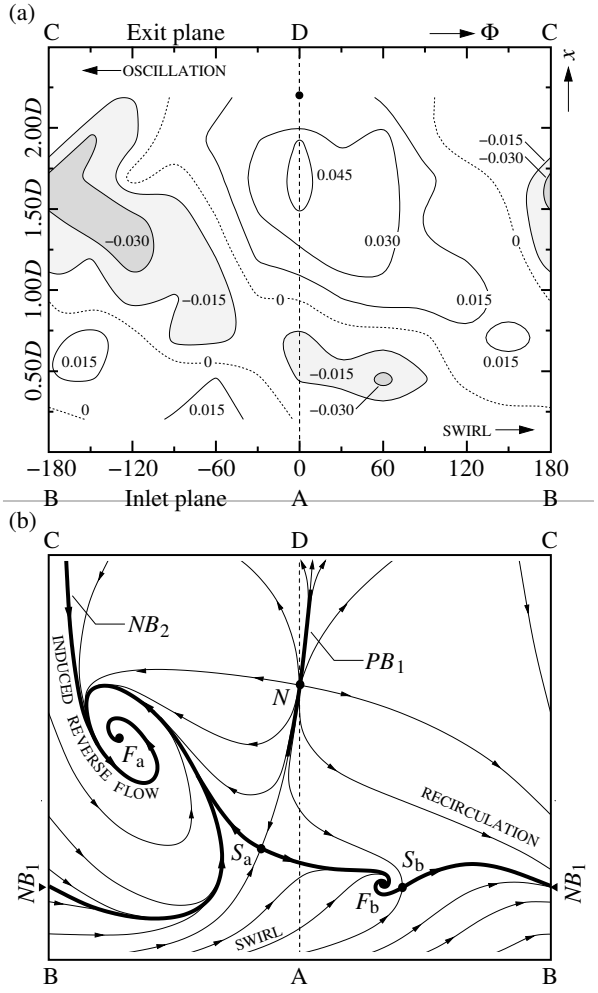

Figure 9: Modified Phillips estimate of the instantaneous wall-pressure distribution of the (downward-deflected) OTJ flow. (a) static-pressure coefficient, P_{wd}/q_1. (b) surface-flow topology inferred by comparing P_{wd}/q_1 with the SDTJ results (Figure 3). $D/d_{e1} = 3.5$, $L/D = 2.50$, $Re_1 = 70{,}000$.

away from this positive bifurcation, converges towards a negative bifurcation NB_2 which, in turn, flows into sink focus/vortex F_a — from both sides of PB_1 because the surface is cylindrical. Low pressure in the vicinity of sink focus F_a is due to centripetal acceleration of flow around the vortex. There is a much smaller region of low pressure at focus F_b.

The surface-flow pattern of the SDTJ, with a chamber length $L = 1.25D$, has a wavy circumferential negative-bifurcation line, NB_1 (Figure 3). Figure 7 indicates that NB_1 is also present in the OTJ flow where the chamber is set to length $L = 2.50D$. However, oscillation of the jet has the effect of time averaging the recorded flow pattern so that NB_1 becomes the plane ring (or a straight line) shown in Figure 7. Since the NB_1 line is present in time-averaged flow-visualisation patterns for both SDTJ and OTJ, we can expect a similar feature in the conditionally-averaged flow pattern of the OTJ. In Figure 9(b), NB_1 is a wavy line located between the OTJ-reattachment point N and the inlet plane $\overline{\text{BAB}}$. As for the SDTJ, this wavy line connects F_a and F_b, the pair of counter-rotating foci. Between the NB_1 line and the inlet plane there is a swirling flow which, from surface-paste visualisation (Figures 3 and 7), travels from left to right (Figure 9(b)).

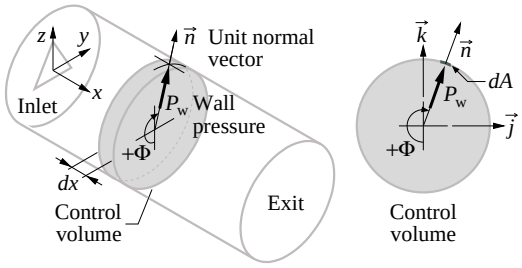

Figure 10: Coordinate system and control-volume definitions.

Estimate of jet deflection

If wall shear stresses are neglected, integrating the wall-pressure (P_w) gives an approximate value of force applied to the flow field by the cylindrical surface (S) of the chamber:

$$F_y = -\iint_S P_w \vec{j}\cdot\vec{n}\ dA, \qquad F_z = -\iint_S P_w \vec{k}\cdot\vec{n}\ dA, \qquad (6)$$

for the coordinate system shown in Figure 10. Unit vectors $\vec{j}$ and $\vec{k}$ are in the y and z coordinate directions (Figure 10), and $\vec{n}$ is the unit outward normal vector on the chamber surface. If we now make the rather crude assumption that the force calculated from Equation 6 is the force acting on the **jet flow only** rather than the whole flow field, we can estimate path of the deflected jet as it passes through the nozzle. Such an estimate is expected to have only an order-of-magnitude accuracy. The first step is to integrate $P_w \vec{j}\cdot\vec{n}$ and $P_w \vec{k}\cdot\vec{n}$ (from Equation 6) around the circumference of the chamber, giving force per unit length as a function of distance x from the inlet plane. Velocity components U_y and U_z of the deflected jet are obtained by applying a momentum balance over the control-volume disc shown in Figure 10. If we make a further approximation $U_x \approx U_1$ along the length of the nozzle, the path (x_s, y_s, z_s) of the deflected jet can be estimated by integrating the streamline,

$$\frac{dy_s}{U_y} = \frac{dx_s}{U_x}, \qquad \frac{dz_s}{U_z} = \frac{dx_s}{U_x}, \qquad (7)$$

starting from $(x_s, y_s, z_s)=(0,0,0)$. The final results, which give deflection as a function of distance x_s from the inlet plane of the OTJ nozzle,

$$\left.\frac{y_s}{D}\right|_{x_s/D} \approx \frac{2}{\pi}\int_0^{x_s/D} \frac{F_y}{\frac{1}{2}\rho {U_1}^2 {d_{e1}}^2}\ d\left(\frac{x'}{D}\right), \qquad (8)$$

$$\left.\frac{z_s}{D}\right|_{x_s/D} \approx \frac{2}{\pi}\int_0^{x_s/D} \frac{F_z}{\frac{1}{2}\rho {U_1}^2 {d_{e1}}^2}\ d\left(\frac{x'}{D}\right), \qquad (9)$$

are shown in Figure 11. The end view in Figure 11(a) shows that the path of the oscillating jet is a counter-clockwise outward spiral. This is consistent with the direction of oscillation inferred from air-bubble visualisation. Estimates of deflection (Figure 11(b)) based on the SDTJ surface-pressure distribution (Figure 3(b)) suggest that the centre of the stationary-deflected jet passes through the shorter cavity with much smaller deflection than the oscillating jet.

Conclusions

Comparison with direct observations demonstrates that a backward-facing pressure sensor placed in the "reattached-flow" region of the oscillating-triangular-jet (OTJ) nozzle is a reliable detector of jet-flow oscillation. With data from the detector probe and simultaneous measurements on the internal

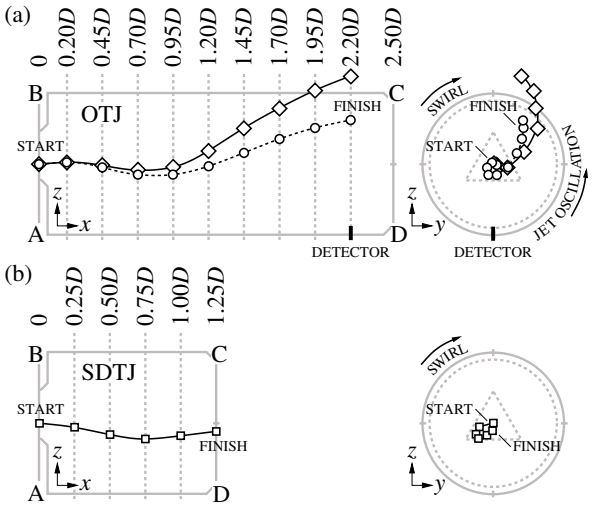

Figure 11: (a) Deflected path of the OTJ is estimated from the conditionally-averaged wall pressure (◇) and the modified Phillips estimate (◯). (b) Deflected path of the SDTJ is estimated from time-averaged wall pressure (□). Deflection in the side view is z_s, and in the downstream view is $\sqrt{{y_s}^2+{z_s}^2}$ (from Equations 8 and 9). $D/d_{e1}=3.5$, $d_2/D=0.9$. $Re_1=70,000$.

surface of the OTJ nozzle, we obtain conditionally-averaged static-pressure distributions by two slightly different methods. Each method gives a similar result — a result which contains the same features as the simple time-averaged pressure distribution produced by the stationary-deflected triangular jet (SDTJ). The inferred OTJ surface-flow topology therefore has the same features as the SDTJ. There is, however, an important difference between the OTJ surface flow and the SDTJ surface flow. For the OTJ, the chamber is twice as long, and the pressure distribution has much greater asymmetry about a mirror plane drawn through the axis of the nozzle and the detector probe. Order-of-magnitude estimates show that the asymmetry is responsible for net side force on the flow through the nozzle. For the OTJ, the force is sufficient to produce significant deflection of the jet flow in directions perpendicular to the nozzle axis.

References

[1] Lee, S. K., Lanspeary, P. V., Nathan, G. J. and Kelso, R. M., Surface-flow patterns in oscillating-triangular-jet nozzles, in *Proceedings of the Fifteenth Australasian Fluid Mechanics Conference*, AFMC00052, Sydney, Australia, 2004.

[2] Lee, S. K., Lanspeary, P. V., Nathan, G. J., Kelso, R. M. and Mi, J., Low kinetic-energy loss oscillating-triangular-jet nozzles, *Experimental Thermal and Fluid Science*, **27**, 2003, 553–561.

[3] Mi, J., Nathan, G. J., Luxton, R. E. and Luminis Pty. Ltd., Naturally oscillating jet devices, Australian Patent Office, Patent Application No. PP0421/97, 1998.

[4] Nathan, G. J., Hill, S. J. and Luxton, R. E., An axisymmetric 'fluidic' nozzle to generate jet precession, *Journal of Fluid Mechanics*, **370**, 1998, 347–380.

[5] Phillips, O. M., Gu, D. and Donelan, M., Expected structure of extreme waves in a Gaussian sea. Part 1: Theory and SWADE buoy measurements, *Journal of Physical Oceanography*, **23**, 1993, 992–1000.

[6] Westerweel, J. and Scarano, F., Universal outlier detection for PIV data, *Experiments in Fluids*, **39**, 2005, 1096–1100.